Using Eulerian and Lagrangian Approaches to Investigate Wind-Driven Changes in the Southern Ocean Abyssal Circulation

PAUL SPENCE AND ERIK VAN SEBILLE

Climate Change Research Centre, and ARC Centre of Excellence for Climate System Science, University of New South Wales, Sydney, New South Wales, Australia

OLEG A. SAENKO

Canadian Centre for Climate Modelling and Analysis, Environment Canada, Victoria, British Columbia, Canada

MATTHEW H. ENGLAND

Climate Change Research Centre, and ARC Centre of Excellence for Climate System Science, University of New South Wales, Sydney, New South Wales, Australia

(Manuscript received 1 May 2013, in final form 4 October 2013)

ABSTRACT

This study uses a global ocean eddy-permitting climate model to explore the export of abyssal water from the Southern Ocean and its sensitivity to projected twenty-first-century poleward-intensifying Southern Ocean wind stress. The abyssal flow pathways and transport are investigated using a combination of Lagrangian and Eulerian techniques. In an Eulerian format, the equator- and poleward flows within similar abyssal density classes are increased by the wind stress changes, making it difficult to explicitly diagnose changes in the abyssal export in a meridional overturning circulation framework. Lagrangian particle analyses are used to identify the major export pathways of Southern Ocean abyssal waters and reveal an increase in the number of particles exported to the subtropics from source regions around Antarctica in response to the wind forcing. Both the Lagrangian particle and Eulerian analyses identify transients as playing a key role in the abyssal export of water from the Southern Ocean. Wind-driven modifications to the potential energy component of the vorticity balance in the abyss are also found to impact the Southern Ocean barotropic circulation.

1. Introduction

The abyssal circulation of the Southern Ocean is often considered, at least in a zonally integrated sense, to consist of two compensating flows. One is associated with the poleward flow of Lower Circumpolar Deep Water (LCDW), and the other is associated with the equatorward flow of Antarctic Bottom Water (AABW) (e.g., Sloyan and Rintoul 2001). LCDW is transformed into AABW by surface buoyancy fluxes at several locations near the Antarctic continental shelf and also through mixing and entrainment processes (Orsi et al. 1999). Observational studies estimate that the Southern Ocean transports distinct varieties of AABW equatorward into the subtropical Atlantic, Pacific, and Indian basins at a net rate of roughly 20 Sverdrups (Sv; $1\,\mathrm{Sv} \equiv 10^6\,\mathrm{m^3\,s^{-1}}$), primarily via a network of deep western boundary currents (DWBCs) (Lumpkin and Speer 2007; Purkey and Johnson 2012). The inflow of LCDW is also thought to occur primarily via DWBCs and is composed of a mixture of North Atlantic Deep Water (NADW) from the Atlantic basin and recirculated deep waters from the Indian and Pacific Oceans (Jacobs 2004; Santoso et al. 2006).

Together, these meridional flows into and out of the Southern Ocean play an important role in the storage and transport of carbon, heat, and other geochemical tracers (e.g., Levitus et al. 2005) and consequently may play a significant role in global climate change (e.g., Meehl et al. 2006). However, understanding the driving mechanisms and predicting these flows is hindered by a number of theoretical and numerical challenges, some of which are addressed here.

Corresponding author address: Paul Spence, Climate Change Research Centre, Level 4, Mathews Building, University of New South Wales, Sydney, NSW 2052, Australia.
E-mail: paul.spence@unsw.edu.au

DOI: 10.1175/JPO-D-13-0108.1

Because of the large domain and circumpolar geometry of the Southern Ocean, its abyssal circulation is commonly interpreted with a meridional overturning circulation (MOC) streamfunction of the zonally integrated transport along isopycnals. However, in this framework it is difficult to determine how the export of AABW from the Southern Ocean is affected by the changing winds. For example, on zonal average, an increased equatorward transport of AABW could be offset by an increased poleward transport of LCDW within similar density classes in the MOC. Furthermore, the Southern Ocean is covered in complex bathymetric features where the local dynamics can be quite different from those described by a zonally integrated framework (e.g., Thompson and Sallée 2012), and the zonal integration hides the network of DWBCs actually responsible for the abyssal transport. In this study, we use a global ocean eddy-permitting climate model and Lagrangian particles to explore the complexities of the volume transport, pathways, and dynamics of abyssal water exported from the Southern Ocean.

Recent theoretical model studies have proposed that the export of abyssal waters from the Southern Ocean is coregulated by wind stress, mesoscale eddies, and diapycnal mixing (e.g., Nikurashin and Vallis 2011; Ito and Marshall 2008). Nikurashin and Vallis (2011) show that the meridional transport in the Southern Ocean abyss can be characterized by two limiting regimes, corresponding to weak and strong diapycnal mixing. In the limit of weak diapycnal mixing, the deep stratification is maintained by the Southern Ocean winds and eddies. In the limit of strong mixing, the abyssal meridional transport is primarily set by eddies and diapycnal mixing, with the winds playing a secondary role.

The real ocean is likely to exist somewhere between these two extremes. In general, stronger mesoscale eddy activity is expected to result in stronger Southern Ocean abyssal export (Olbers and Ivchenko 2001; Ito and Marshall 2008). Furthermore, assuming that the energy maintaining the diapycnal mixing is supplied, at least in part, by the winds (either directly or through the mesoscale eddies), the effects of diapycnal mixing, mesoscale eddies, and winds on the meridional transport of the deep Southern Ocean becomes difficult to separate (Saenko et al. 2012). In such a case, the whole system is essentially controlled by the wind: wind steepens the isopycnals and generates mesoscale eddies, and the eddies generate small-scale mixing that drives the export of abyssal water from the Southern Ocean.

Here, we focus on the effects of winds, and in particular, the impact of projected twenty-first-century changes in Southern Hemisphere zonal winds on the export of abyssal water from the Southern Ocean. We also evaluate the role of temporal variability in the Southern Ocean abyssal transport and explore its response to projected anthropogenic changes in wind stress.

Atmospheric observations reveal a poleward intensification of Southern Hemisphere westerly winds since the 1950s, identified as a positive shift in the southern annular mode (SAM), which has been attributed to increasing atmospheric concentrations of ozone-depleting and greenhouse gases (Thompson et al. 2011). Global climate models are remarkably consistent in simulating a continuation of the observed positive SAM trend throughout the twenty-first century (Fyfe et al. 2007). A positive SAM trend has been shown to increase the outflow of NADW from the North Atlantic and enhance the upwelling of LCDW in the Southern Ocean (Oke and England 2004; Russell et al. 2006).

In a set of 16 coarse-resolution climate models evaluated by Saenko et al. (2012), all but one model predicts a stronger time-mean poleward flow between 55° and 60°S averaged over the bottom 1000 m (for depths $>$3000 m) in a warmer twenty-first-century climate accompanied by a positive SAM trend. This may be expected because the SAM trend increases the equatorward surface Ekman transport, which is balanced in a zonally averaged sense by a poleward-mean geostrophic flow below the sill depths across Drake Passage (Munk and Palmén 1951). However, it has been argued that wind-driven changes in the time-mean transport could be largely compensated by changes in the transient-driven transport (Hallberg and Gnanadesikan 2006).

Saenko et al. (2012) also briefly evaluated the Southern Ocean abyssal MOC response to a projected twenty-first-century SAM trend with a global ocean eddy-permitting climate model. A zonally integrated, latitude-density MOC framework provides useful information on the diapycnal transformation from dense to lighter waters. Using this framework, Saenko et al. (2012) found that the transient overturning points to an increase in the Southern Ocean abyssal export under projected twenty-first-century wind changes, while the residual circulation points to a net decrease. However, as discussed above, in this zonally integrated framework it remains unclear how the export of AABW from the Southern Ocean is affected by the changing winds. It is also reasonable to ask how much of the exported AABW recirculates back to the Southern Ocean without getting converted to the lighter waters, which is also discussed here.

In this study, we investigate the export of Southern Ocean abyssal water in the global eddy-permitting climate model briefly discussed in Saenko et al. (2012) using both Lagrangian and Eulerian frameworks. In the Eulerian framework, the meridional components (i.e.,

equatorward and poleward) of the zonally integrated abyssal transport by the time-mean and transient circulations are evaluated. We also integrate the abyssal transport along Antarctic Circumpolar Current (ACC) streamlines, separately evaluating the positive and negative across-streamline components (i.e., equatorward or poleward) of both the time-mean and transient circulations. Lagrangian particle analyses are used to reveal the abyssal transport pathways of water exported from the Southern Ocean in the model, clarify the role of transient circulations in the export, and estimate changes in the formation regions of Southern Ocean abyssal water in response to projected twenty-first-century wind stress changes. The Southern Ocean potential vorticity (PV) balance (refer to the appendix for details on the PV theory) is also used to explore the dynamical mechanisms maintaining the abyssal transport pathways and the impact of wind-driven changes in the density of the abyssal waters on the Southern Ocean circulation.

2. Numerical models and experimental design

a. The Earth system climate model

This study uses the University of Victoria Earth System Climate Model (ESCM). It couples a vertically integrated energy–moisture balance atmospheric model, a thermodynamic–dynamic sea ice model, and a land surface model with the Geophysical Fluid Dynamics Laboratory Modular Ocean Model (Weaver et al. 2001).

Here, the oceanic component has an eddy-permitting horizontal resolution of $0.2° \times 0.4°$ (latitude $\times$ longitude). This corresponds to a resolution of about 25 km at 60°S, which is larger than typical local values of the first baroclinic Rossby radius. We note, however, that medium-sized mesoscale eddies identified from satellite altimetry, including those in high latitudes, have characteristic diameters on the order of 100 km (Chelton et al. 2007), so that the model can be considered ocean eddy permitting. The model was equilibrated for 100 years, starting from a 3000-year equilibrium state of a $1.8° \times 3.6°$ model version. This allows us to evaluate deep ocean flows in a near-equilibrium state of a coupled global climate model without idealized buoyancy fluxes or boundary conditions. The model was equilibrated under fixed year 1900 radiative forcing conditions.

As discussed in Saenko et al. (2012), two ESCM simulations are analyzed: a control (CNTRL) and a wind perturbation (WIND) simulation. In CNTRL, the wind stress corresponds to the National Centers for Environmental Prediction (NCEP)–National Center for Atmospheric Research (hereafter referred to as NCEP; Kistler et al. 2001) reanalysis climatology. The WIND simulation is identical to the CNTRL, except that poleward-intensifying wind anomalies projected for the years 2061–2100 have been added to the CNTRL wind stress in the Southern Ocean as a transient perturbation. Atmospheric buoyancy fluxes, sea ice, and the ocean can all be impacted by the applied wind forcing.

The wind anomalies were assembled from simulations performed by 10 different global climate models from phase 3 of the World Climate Research Programme (WCRP) Coupled Model Intercomparison Project (CMIP3) multimodel ensemble (forced by the same CO_2 trajectory; see Fyfe et al. 2007). In WIND, the anomalies are added directly to the NCEP reanalysis wind climatology used in CNTRL. The WIND forcing [not shown; see Fig. 7 in Fyfe et al. (2007)] is such that the CNTRL zonal wind stress increases south of 50°S by a maximum of about 20% accompanied by roughly a 3° poleward shift. While applying wind anomalies only in the Southern Hemisphere disturbs the global momentum balance, it allows the impacts of the projected positive SAM trend to be investigated.

Previous studies based on the CNTRL simulation have shown that the large-scale ocean transports [e.g., Drake Passage transport (Spence et al. 2009) and Atlantic meridional overturning transport (Spence et al. 2013)] in CNTRL are steady. The time series of the annual-mean AABW transport in CNTRL is also steady at -13.1 Sv with a standard deviation of 1.2 Sv. The equilibration of ocean tracer fields over millennia will lead to long-term drift in the velocity fields. All results presented use output from the last 5 years of the simulations, and model drift is accounted for in any anomalies presented, at least in a linear sense, by differencing the WIND simulation from the concomitantly extended CNTRL simulation. We also conducted the CNTRL simulation analysis (Lagrangian and Eulerian) at years 100 and 140, finding no significant difference in the results.

b. Lagrangian particle model

Recently, van Sebille et al. (2013) used the Connectivity Modeling System (Paris et al 2013) to track the transport pathways of AABW from its formation regions around Antarctica to the deep subtropical basins with virtual Lagrangian floats driven by the velocity field of the Southern Ocean State Estimate model (SOSE; Mazloff et al. 2010). Here, we use a similar methodology to identify the transport pathways of Southern Ocean abyssal water into the subtropical basins in the high-resolution ESCM, with a focus on identifying the role of transients in the export and revealing how the pathways respond to projected twenty-first-century wind stress changes. Given that SOSE is highly constrained by a large set of in situ and remotely sensed observations,

van Sebille et al. (2013) were able to explicitly identify AABW particles by following an observationally consistent classification based on neutral density.

The fully coupled ESCM used in this study evolves without ocean observation constraints. Consequently, the Southern Ocean abyssal water masses do not strictly meet the observationally based neutral density classifications of AABW. Consequently, we refrain from explicitly identifying particles as AABW in ESCM and generalize the Lagrangian particle analysis to the export of abyssal waters from the Southern Ocean. In this study, the Lagrangian particles are released at 18.5-m depth poleward of 60°S, and only those particles that reach depths greater than 3500 m before reaching the typical base of the mixed layer (~150 m) north of 30°S are taken into account.

The Lagrangian particles are driven by the three-dimensional ESCM velocity field for a maximum of 1000 years. The Lagrangian particles are released on a 2° × 2° grid poleward of 60°S at 18.5-m depth every 5 days during 1 year. This means that a total of 78 597 particles are released. After being released, the particles are advected using the full three-dimensional ESCM velocity fields on 5-day resolution, employing a fourth-order Runge–Kutta-type advection scheme as implemented in the Connectivity Modeling System. The particles can thus change depths as they follow the water mass pathways.

Only five years of velocity data are available, so in order to extend the length of the particle integration, the velocity fields are looped so that every five years the time series is recycled, allowing us to track the particles for centuries. Van Sebille et al. (2012) successfully used this looping methodology to track North Atlantic particle pathways for several centuries. The particle locations are saved every two weeks. Note that the interpretation of the particle trajectories in this case is slightly different from the traditional idea of them carrying water around the ocean. The Lagrangian particle trajectories are best interpreted as tracing a Lagrangian streamfunction [see for example the work by Döös et al. (2008)]. The Lagrangian particles thus provide a perspective of the flow pathways that complements the Eulerian streamfunctions. The different trajectories generated by the WIND and CNTRL simulations are used to indicate AABW pathway changes induced by the wind anomalies.

3. Results

a. Eulerian transport analysis

The Ekman transport associated with the westerly wind stress over the Southern Ocean results in a mean northward transport $\overline{\Psi}$, which is partially compensated by an opposing eddy-induced transport Ψ^* (Marshall and Radko 2003). The residual (or total) overturning is the sum of the mean and eddy-induced transports ($\Psi_{\mathrm{RES}} = \overline{\Psi} + \Psi^*$). Figure 1 shows the zonally integrated Ψ_{RES} for both the WIND and CNTRL simulations. The streamfunctions are plotted as a function of potential density referenced to 3000-m depth σ_3 to elucidate the transport of abyssal waters by the lower-cell component of the MOC [refer to Spence et al. (2009) for details on the streamfunction calculations]. The Ψ_{RES} has a maximum equatorward transport of 27 Sv between 60° and 65°S for $\sigma_3 > 41.7\,\mathrm{kg\,m^{-3}}$ in CNTRL (the mean depth of $\sigma_3 = 41.7\,\mathrm{kg\,m^{-3}}$ around 55°S in CNTRL is about 2395 m, reaching locally to more than 4000-m depth). Between 55° and 60°S, the transient circulation is responsible for roughly 10 Sv of the equatorward transport for $\sigma_3 > 41.4\,\mathrm{kg\,m^{-3}}$ in CNTRL. Most of the transient transport takes place within the densest water classes (i.e., around $\sigma_3 = 41.8\,\mathrm{kg\,m^{-3}}$). In the WIND simulation the maximum intensity of the lower-cell Ψ_{RES} transport decreases by 8 Sv, while the transient overturning intensifies by as much as 9 Sv relative to CNTRL. Most of the intensification of the transient transport takes place for $\sigma_3 < 41.7\,\mathrm{kg\,m^{-3}}$. However, for $\sigma_3 > 41.7\,\mathrm{kg\,m^{-3}}$ there is also an increase of 1–3 Sv in the equatorward transport by the transient overturning at most latitudes between 50° and 60°S.

The intensification of the transient overturning thus points to an increase in the Southern Ocean abyssal export under projected twenty-first-century wind changes, while the residual circulation points to a net decrease. In this framework, it remains unclear how the export of AABW from the Southern Ocean is affected by the changing winds. For example, an increased equatorward transport of AABW could be offset by an increased poleward transport of LCDW within similar density classes in the residual MOC. Alternatively, an increased equatorward transport of AABW by the transient circulation could be offset by a decrease in the equatorward transport of AABW by the time-mean circulation.

We further explore these complexities by considering the transport within the bottom half of the lower-cell MOC and across the barotropic streamlines of the ACC to exclude the transport due to permanent meridional excursions of the ACC (or standing eddies). The time-mean abyssal flows tend to be aligned with the time-mean barotropic ACC streamlines (Fig. 2). However, there are reasons to think (Krupitsky and Cane 1997) that the flows in the upper Southern Ocean (below the Ekman layer) should follow the net barotropic streamfunction more closely than the flows in the abyss, where

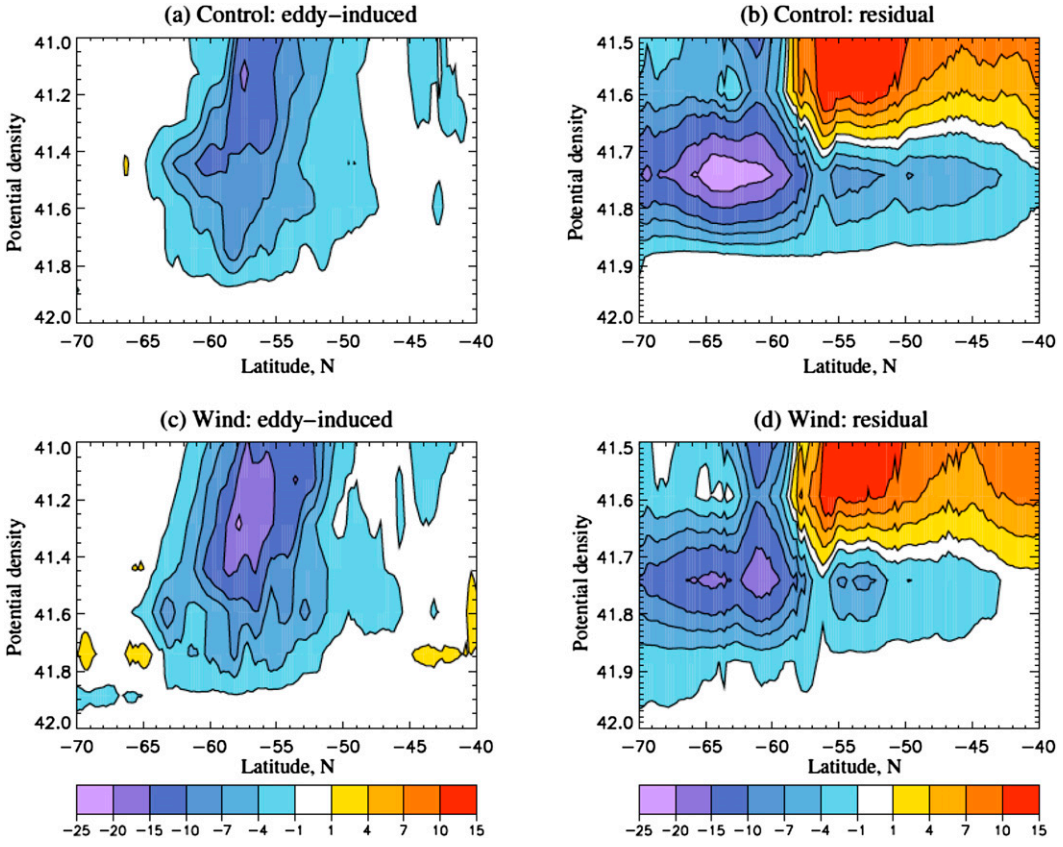

FIG. 1. Overturning circulation (Sv) in the Southern Ocean as a function of potential density referenced to 3000-m depth (i.e., σ_3) in the (a),(b) control and (c),(d) wind experiments: transient Ψ (left) and residual Ψ_{RES} (right) transport within the densest water classes. Negative values indicate counterclockwise circulation. Note that the vertical scale in (b) and (d) is only half of that in (a) and (c). Reproduced from Saenko et al. (2012).

they are more affected by the topography. Hence, there can be cross-stream flows, as discussed below.

Figure 3 shows the time-mean and transient across-streamline transport accumulated by following along ACC streamlines for waters with $\sigma_3 \geq 41.75\,\mathrm{kg\,m^{-3}}$ ($\sigma_3 = 41.75\,\mathrm{kg\,m^{-3}}$ is the density within the core of the residual lower-cell MOC in Fig. 1b). For simplicity, we discuss the across-streamline transport as meridional relative to the time-mean latitudinal position of the ACC streamline. In CNTRL, the time-mean transport across ACC streamlines is equatorward for streamlines with zonal-mean latitudes equatorward of 57°S and poleward for streamlines with a mean position south of 57°S. In WIND, there is more poleward (or less equatorward) time-mean across-streamline transport and the transition from a poleward to equatorward time-mean transport is shifted equatorward to streamlines with a zonal-mean latitude of 55°S. The transient meridional transport across ACC streamlines is predominately equatorward in both WIND and CNTRL, and transient transport is larger in magnitude than the time-mean transport for streamlines with a mean position south of 54°S. In WIND there is a 5–9 Sv increase in the along streamline transient transport south 55°S (90-Sv streamline) and a 0–3 Sv decrease between 52° and 55°S (90-Sv streamline), followed by a 4 Sv increase at 51°S.

The cross-stream transport following any ACC streamline is composed of positive and negative components. We define positive components as directed toward the equatorward side of the ACC and negative components as directed toward the poleward side of the ACC. Table 1 shows the positive and negative components of the time-mean and transient across-streamline transports accumulated along the 100-Sv streamline. The time-mean transport across the 100-Sv streamline in CNTRL accumulates to 3.98-Sv transport that is composed of a 38.61-Sv negative (poleward) flow and a 42.59-Sv positive (equatorward) flow. Similarly, the transient transport in CNTRL accumulates to 7.68-Sv positive (equatorward) transport that is composed of a 0.02-Sv negative (poleward) transport and a 7.70-Sv positive (equatorward) transport. In response to the

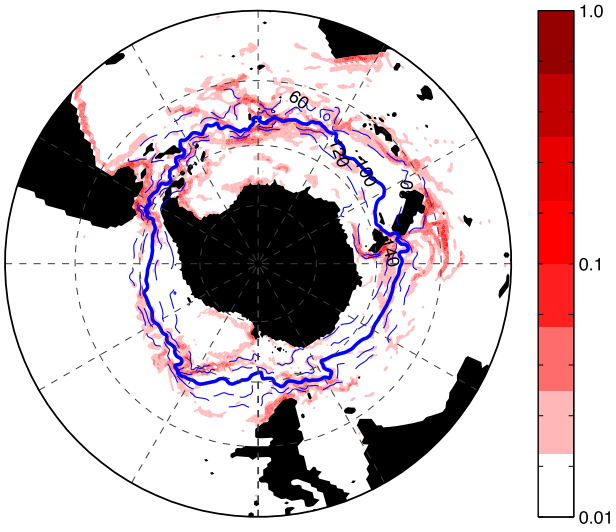

FIG. 2. The time-mean speed (m s^{-1}) of the flow depth averaged below 2000-m depth. Contours of barotropic streamfunction are plotted in blue from $\psi = 60$ to 140 Sv with 20-Sv contour intervals and the 100-Sv line in boldface. In general, the deep flow aligns well with this barotropic streamfunction, which allows us to meaningfully calculate deep transports across these streamfunctions.

WIND forcing, the positive and negative across-streamline transport components are increased in both the time-mean and transient circulations (Table 1). If one ignores local recirculations and associates the poleward-flowing abyssal water with LCDW and the equatorward-flowing water with AABW, then these results suggest that the wind forcing generates large increases in the abyssal transport by the time-mean and transient circulations of both water masses.

b. *Lagrangian particle analysis*

The analysis of the meridional transport in the previous section showed that the decrease in the residual abyssal MOC transport induced by the WIND forcing is the net result of larger and compensating changes in the pole- and equatorward flows within both the time-mean and transient circulations. However, the abyssal transport pathways cannot be identified in the MOC transports, and one may question to what extent these changes are the result of local recirculations of abyssal waters.

To address these issues, we identified the transport pathways of Southern Ocean abyssal water from its source regions around Antarctica to the subtropical basins using Lagrangian particles. Such Lagrangian particles have been successfully used before by, for example, Döös et al. (2008) to study pathways of water and the associated Lagrangian streamfunctions of the Southern Ocean in a numerical ocean model. Here, the particles are driven by 5-day snapshots of the ESCM velocity fields. Recall from section 2b that the particles are released at 18.5-m depth poleward of 60°S, and only those particles that reach depths greater than 3500 m before reaching the typical base of the mixed layer (~150 m) equatorward of 30°S are taken into account.

Three major pathways equatorward from the Antarctic coast can be observed from the trajectories of the Lagrangian particles: from the Weddell Sea, from the Ross Sea south of New Zealand, and from Prydz Bay near 60°E [Fig. 4 (left)]. These particles tend to veer eastward under the Antarctic Circumpolar Current north of 40°S and become more diffusive downstream as

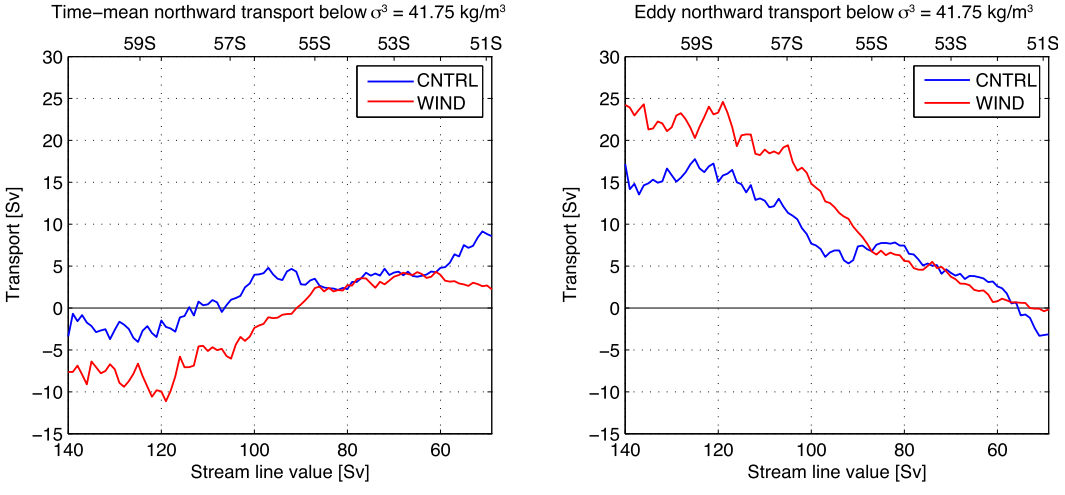

FIG. 3. Eulerian analysis of the transport (Sv) across ACC streamlines and below the $\sigma_3 = 41.75$ kg m^{-3} isopycnal, which is the core of the lower-cell MOC. The (left) time-mean transport and (right) transient-induced transport. The top x axis provides the mean lat of the ACC streamlines shown on the bottom x axis.

TABLE 1. Abyssal volume transport across the 100-Sv ACC streamline. The time-mean and transient components of the volume transport across the 100-Sv ACC streamline for water with $\sigma_3 \geq 41.75\,\mathrm{kg\,m^{-3}}$ ($\sigma_3 = 41.75\,\mathrm{kg\,m^{-3}}$ is the density within the core of the residual lower-cell MOC in Fig. 1b). The time-mean and transient transports are separated into positive and negative components for both the WIND and CNTRL simulations. The positive components are directed toward decreasing ACC transport (generally equatorward) and negative components are directed toward increasing ACC transport (generally poleward).

	WIND	CNTRL	Anomaly
Time-mean (Sv)	−2.37	3.98	−6.34
Positive (equatorward) time-mean component (Sv)	50.58	42.59	7.99
Negative (poleward) time-mean component (Sv)	−52.95	−38.61	−14.34
Transient (Sv)	14.84	7.68	7.16
Positive (equatorward) transient component (Sv)	16.58	7.70	8.88
Negative (poleward) transient component (Sv)	−1.74	−0.02	−1.72

mixing spreads the abyssal particles horizontally. The particles cross into the Atlantic by following the Scotia Ridge downstream of the Drake Passage. The dominant pathways into the Pacific basin are found off the east coast of Tasmania and the west coast of South America. The Indian Basin pathways are found near the Kerguelen Plateau and the Southwest Indian Ridge. The time for particles to reach 45°S at depths below 3500 m in both CNTRL and the SOSE estimate (van Sebille et al. 2013) is less than 200 yr.

The dominant particle pathways across 55°S are in general agreement with observations (Orsi 2010; Purkey and Johnson 2012) and the trajectory analysis of van Sebille et al. (2013) in the SOSE. While the abyssal pathways in SOSE and ESCM are similar, there are notable differences in the percentage of particles exported to each subtropical basin. In SOSE, ~70% of the particles identified as AABW end up in the Pacific Ocean, ~25% of the particles end up in the Indian Ocean, and ~7.5% of the particles end up in the Atlantic Ocean. In ESCM, we find that 31% of abyssal particles exported end up in the Pacific Ocean, 29% end up in the Indian Ocean, and 31% end up in the Atlantic Ocean. These differences can be at least partly attributed to the different methods used to identify abyssal particles and the unconstrained climatology of ESCM.

To illustrate the role of transient processes in exporting abyssal particles out of the Southern Ocean in the Lagrangian framework, we use monthly-mean velocity fields from the CNTRL simulation to drive the particles rather than 5-day snapshots [Fig. 4 (right)]. When driven by monthly-mean velocity fields, the particle trajectories are to a large extent limited to large cyclonic gyres in the Ross and Weddell Sea regions with very few particles leaving the Southern Ocean. Consistent with the strength of the transient equatorward volume flux shown in Fig. 1a, this implies a crucial role for transients in the abyssal transport of water out of the Southern Ocean.

In an effort to quantify the local recirculation of abyssal particles, we calculated the fraction of particles that recirculate back across an ACC streamline before leaving

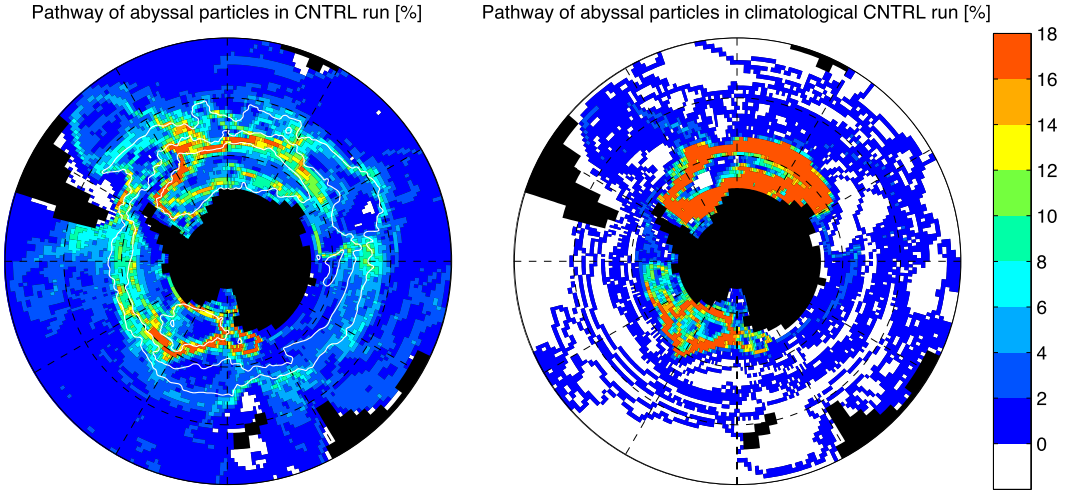

FIG. 4. The abyssal pathway of water formed near the Antarctic coast as reconstructed from the trajectories of all Lagrangian particles released south of 60°S that reach depths below 3500 m south of 30°S. (left) Trajectories driven by 5-day snapshots of the CNTRL simulation velocity field. (right) Trajectories driven by monthly-mean CNTRL simulation velocity fields. The pathways are determined from the trajectories of the 2023 AABW particles, where for each 0.5° × 0.5° grid cell the probability (%) is given that it is crossed by a particle. The white lines (left) are three barotropic streamlines of the ACC.

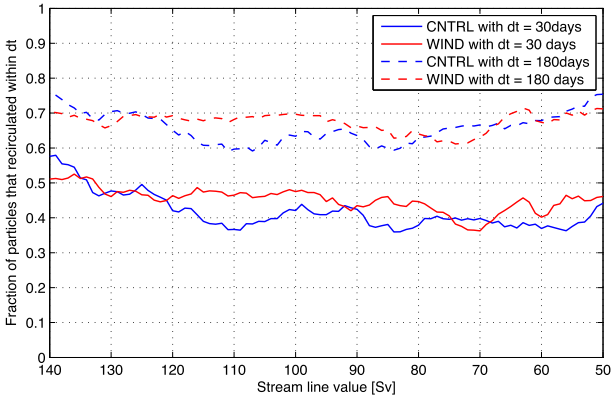

FIG. 5. The fraction of abyssal particles that after crossing an ACC streamline recirculate back across the same streamline within a certain time frame *dt* before being exported from the Southern Ocean.

the Southern Ocean (Fig. 5). A particle with an average abyssal velocity of 0.2 m s^{-1} travels 8.6 km in 30 days. A 30-day time scale is often considered as an upper limit for diagnosing the Eulerian eddy-induced streamfunction. In CNTRL, within 30 (180) days after crossing an ACC streamline ~40% (~65%) of the exported abyssal particles recirculate back across the same streamline. In response to the WIND forcing, the recirculated particle fraction generally increases (by as much as ~10%), irrespective of the time scale. In the WIND simulation, the number of abyssal particles identified also increases by 11%. This is in agreement with the increased equatorward volume flux in the abyssal portion of the residual circulation that is accomplished by the transient circulation component (see Fig. 1 and also Table 1). We also note that instead of an 11% increase in number of abyssal particles meeting our classification, the Lagrangian model produces a 7% decrease when the monthly-mean velocity fields are used in the WIND experiment, again demonstrating the crucial role of the transient circulation in setting the AABW transport strength and pathways in the model.

Despite the net increase in number of abyssal particles exported from the Southern Ocean in response to the WIND forcing, changes in their source regions are not spatially uniform (Fig. 6). Of all the particles identified in the CNTRL run, 39% are formed in the Ross Sea, 26% in the Weddell Sea, 16% in the region between those two seas to the west of the peninsula, and the remaining 18% is formed on the eastern side of Antarctica. In the WIND simulation, the number of particles identified increases by up to 25% in the Weddell Sea, and there are also large increases in the Ross Sea and the Cape Darnley polynya. On the other hand, there is a general decrease in abyssal particle formation on the western side of the Antarctic Peninsula. Although the absolute numbers of particles that form AABW are relatively low (in the order of 2000 particles), these numbers are quite robust. When taking a random subset of half of all particles released, the relative number of particles that form AABW, as well as their spatial distribution, is very similar to that in Fig. 6 (not shown). The AABW source regions indicated by the Lagrangian trajectories (Fig. 6) are in agreement with the Eulerian convective source regions. Changes in the abyssal particle pathways induced by the wind forcing are shown in Fig. 7. It reveals a general intensification of the export pathways in response to the wind forcing, except off the coast of the Ross Sea where a decrease is found.

c. *Dynamical considerations*

The previous section revealed the principal Southern Ocean pathways of the abyssal transport in ESCM and

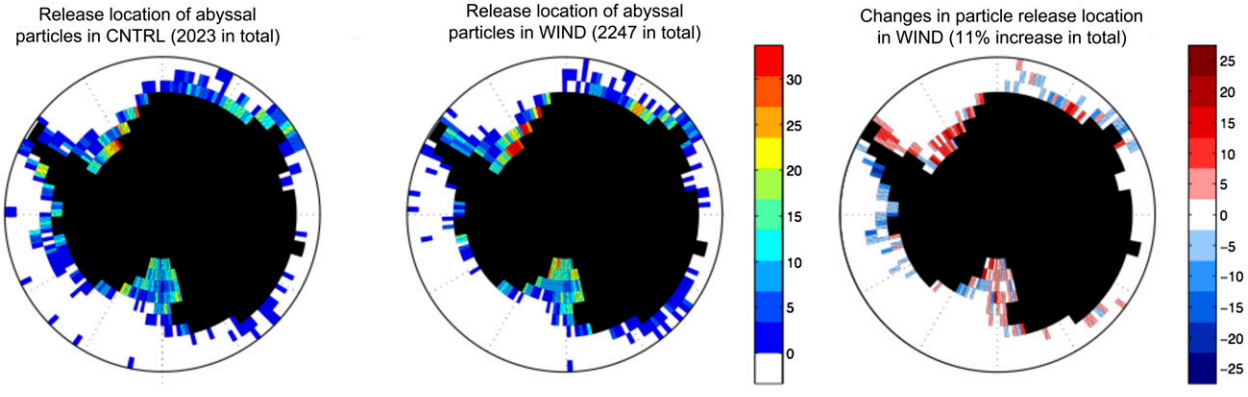

FIG. 6. The location where abyssal water is formed near Antarctica, defined as the number of particles per grid box that reach depths below 3500 m south of 30°S in the (left) CNTRL run, (middle) WIND run, and (right) WIND − CNTRL anomaly. The amount of abyssal particles increases by 11% in the WIND run, as compared to CNTRL. Most of that increase happens in the Ross and Weddell Seas, as well as at 60°E. However, there is considerable decrease of abyssal water formation in the WIND run on the western side of the peninsula.

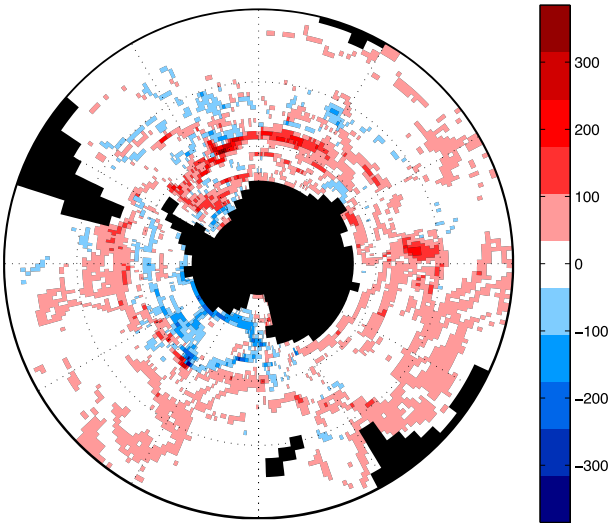

FIG. 7. Changes in the Lagrangian pathways of abyssal waters formed near Antarctica induced by the wind forcing, defined as the difference between WIND and CNTRL in the number of particles per 0.5° × 0.5° grid cell released south of 60°S that reach depths below 3500 m south of 30°S. Units are the number of particles.

their response to the WIND forcing. We now consider the potential vorticity dynamics maintaining the Southern Ocean abyssal transport (refer to the appendix for theoretical considerations).

On zonal mean $\psi_x = 0$, where ψ is the barotropic circulation, and as follows from Eq. (A7) (see the appendix), the zonal-mean wind stress curl must be balanced by bottom pressure torque (BPT). Figure 8 (top) shows the CNTRL simulation Southern Ocean BPT, estimated as $-\rho_0 f w_B$, where w_B is the vertical velocity through the top of grid cells located directly above the seafloor, ρ_0 is a reference density, and f is the Coriolis parameter. The simulated BPT is noisy with absolute values on the order of $10^{-6}\,\mathrm{N\,m^{-3}}$ and with $|w_B| \approx 10^{-5}\,\mathrm{m\,s^{-1}}$ not uncommon. The noisiness can be attributed to large spatial gradients in bottom stress that can be exacerbated by artificially large nonlinear and viscous forces generated by a coarse vertical resolution of bottom topography, especially near large seafloor terraces. Regardless, the spatial pattern of BPT resembles the abyssal particle pathways. There is a pointwise correlation of 0.32 between Figs. 4 (left) and 8 (top), in agreement with the suggestion of Hughes and Cuevas (2001) and Spence et al. (2012) that BPT plays an important role in maintaining the abyssal transport in high-resolution simulations. Indeed, Spence et al. (2012) identified BPT as a key component in maintaining meridional abyssal flows in the interior North Atlantic in the CNTRL simulation. A smoothed version of the BPT field [Fig. 8 (bottom)] clarifies a tendency for large negative BPT values to be

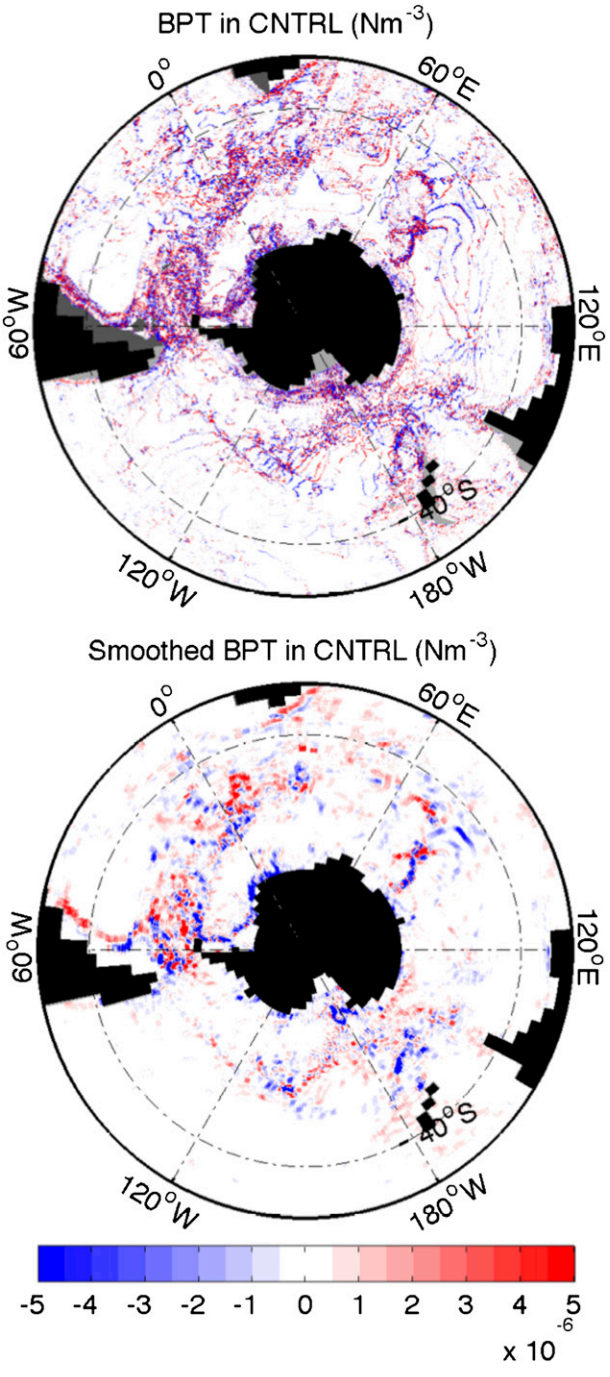

FIG. 8. (top) CNTRL annual-mean bottom pressure torque estimated as $-\rho_0 f w_B$ ($10^{-6}\,\mathrm{N\,m^{-3}}$). (bottom) As in (top) but for values smoothed via an area-mean filter.

positively (negatively) correlated with the equatorward (poleward) flows.

Hughes and Cuevas (2001) present a convincing theoretical argument, confirmed by an eddy-permitting GCM simulation, that for zonal strips of a few degrees latitude, the dominant balance in the area-integrated barotropic

vorticity equation is the wind stress curl and bottom pressure torque in the Southern Ocean (and elsewhere). Assuming that a representative value for the large-scale horizontal velocity near the bottom $|\mathbf{u}_B|$ is $10^{-2}\,\mathrm{m\,s^{-1}}$ and using $|\nabla D| = 10^{-3}$ as a representative value for the magnitude of large-scale bottom topographic slopes, the associated near-bottom vertical velocity $|w_B| = |\mathbf{u}_B||\nabla D|$ can be as large as $10^{-5}\,\mathrm{m\,s^{-1}}$. This is an order of magnitude larger than typical values of surface Ekman pumping. It is also much larger than typical values of mixing-driven upwelling (assuming for the latter a vertical diffusivity of $10^{-4}\,\mathrm{m^2\,s^{-1}}$ acting over a corresponding vertical scale of 10^3 m). While the above estimate for $|w_B|$ is biased toward its upper limit (because the cross-slope component of $\mathbf{u}_B$ is likely to be generally smaller than $|\mathbf{u}_B|$), it does suggest that the effect of bottom pressure torques can be very important. We further note that the BPT signature and the number of abyssal Lagrangian particles exported into the subtropics are greatly reduced in a coarse (>1°)-resolution simulation (not shown) that requires a higher horizontal viscosity for numerical stability.

However, locally the direct influence of the wind stress curl in the Southern Ocean PV budget is small, and the dominant terms in Eq. (A8) (see the appendix), by roughly an order of magnitude, are the topographic planetary Jacobian $J(\psi, f/H)$ and joint effect of baroclinicity and bottom relief (JEBAR) terms (e.g., Hughes and de Cuevas (2001); Borowski et al. 2002; Sarkisyan (2006); Olbers et al. 2007). As pointed out by Borowski et al. (2002), if one neglects the local wind stress curl, then the local PV balance of Eq. (A8) can be reduced to $\psi \approx \tilde{E}/f$, where $\tilde{E} = g/\rho_0 \int_{-H}^{0} (\rho - \overline{\rho}) z\, dz$, with $\rho(x, y, z)$ and $\overline{\rho}(z)$ being the potential density and its globally averaged profile, respectively. Figure 9 provides a comparison of $\tilde{E}/f$ in ESCM with the Locarnini et al. (2010) and Antonov et al. (2010) observational estimate. The magnitude of $\tilde{E}/f$ tends to be weaker in ESCM than observed, but the spatial patterns are consistent. The differences can be attributed to the models' density field diverging from the observational estimate used for initial conditions. Note that the $\tilde{E}/f$ transport resembles the barotropic streamfunction ψ shown in Fig. 2.

By following Borowski et al. (2002) and neglecting the wind stress curl term in Eq. (A8), changes in the Southern Ocean PV balance can be reduced to $\Delta\psi \approx \Delta\tilde{E}/f$. The WIND forcing may indirectly influence the barotropic circulation by altering the $(\rho - \overline{\rho})$ term of $\tilde{E}$. Density changes in the abyss may be particularly important because of the dependence of $\tilde{E}$ on depth. Figure 10 shows $\Delta\tilde{E}/f$ integrated over the full water depth and below 1500 m, along with $\Delta\psi$ induced by the WIND forcing. While the magnitude of $\Delta\psi$ is generally larger, the spatial pattern is consistent with $\Delta\tilde{E}/f$. Both decrease between

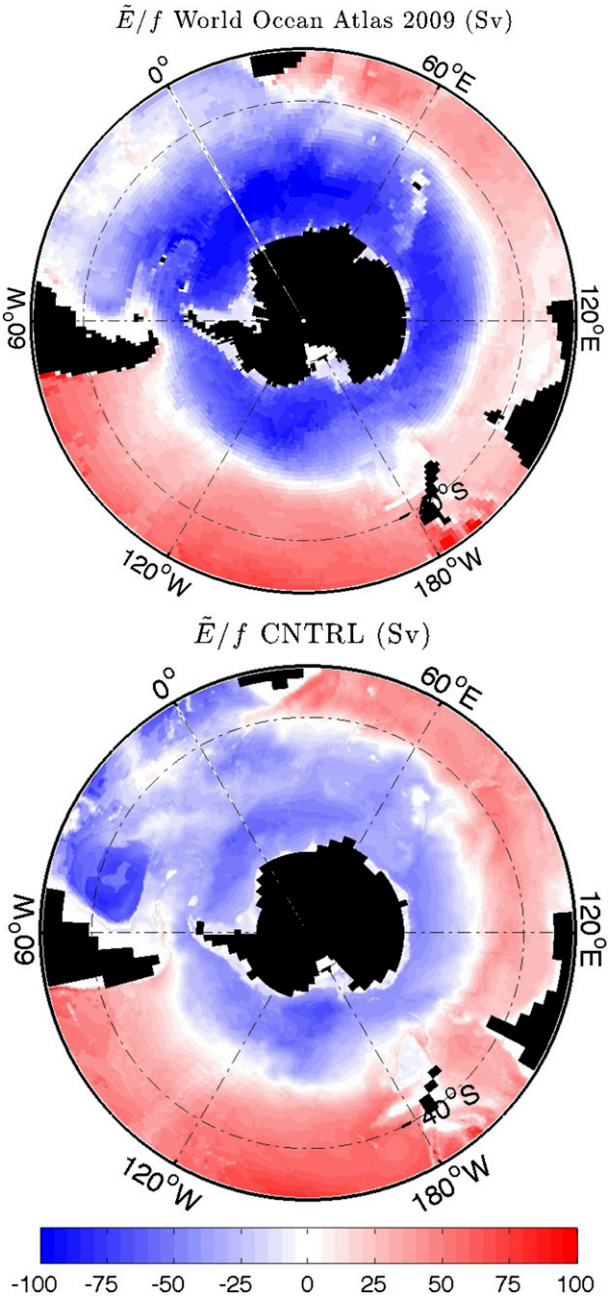

FIG. 9. (top) The $\tilde{E}/f$ in the Locarnini et al. (2010) and Antonov et al. (2010) datasets, and (bottom) averaged over the last 5 years of the CNTRL simulation. $\tilde{E} = g/\rho_0 \int_{-H}^{0} (\rho - \overline{\rho}) z\, dz$. Units are Sv.

roughly 40° and 55°S and increase at higher and lower latitudes, a pattern that resembles the changes in Ekman pumping. The pointwise correlation coefficient between $\Delta\psi$ and $\Delta\tilde{E}/f$ in Fig. 10 is 0.52 when E is integrated over the full depth, and 0.32 when E is integrated over the bottom 1500 m.

This is not the first study to illustrate the connection between the spatial pattern of $\Delta\tilde{E}/f$ and the barotropic

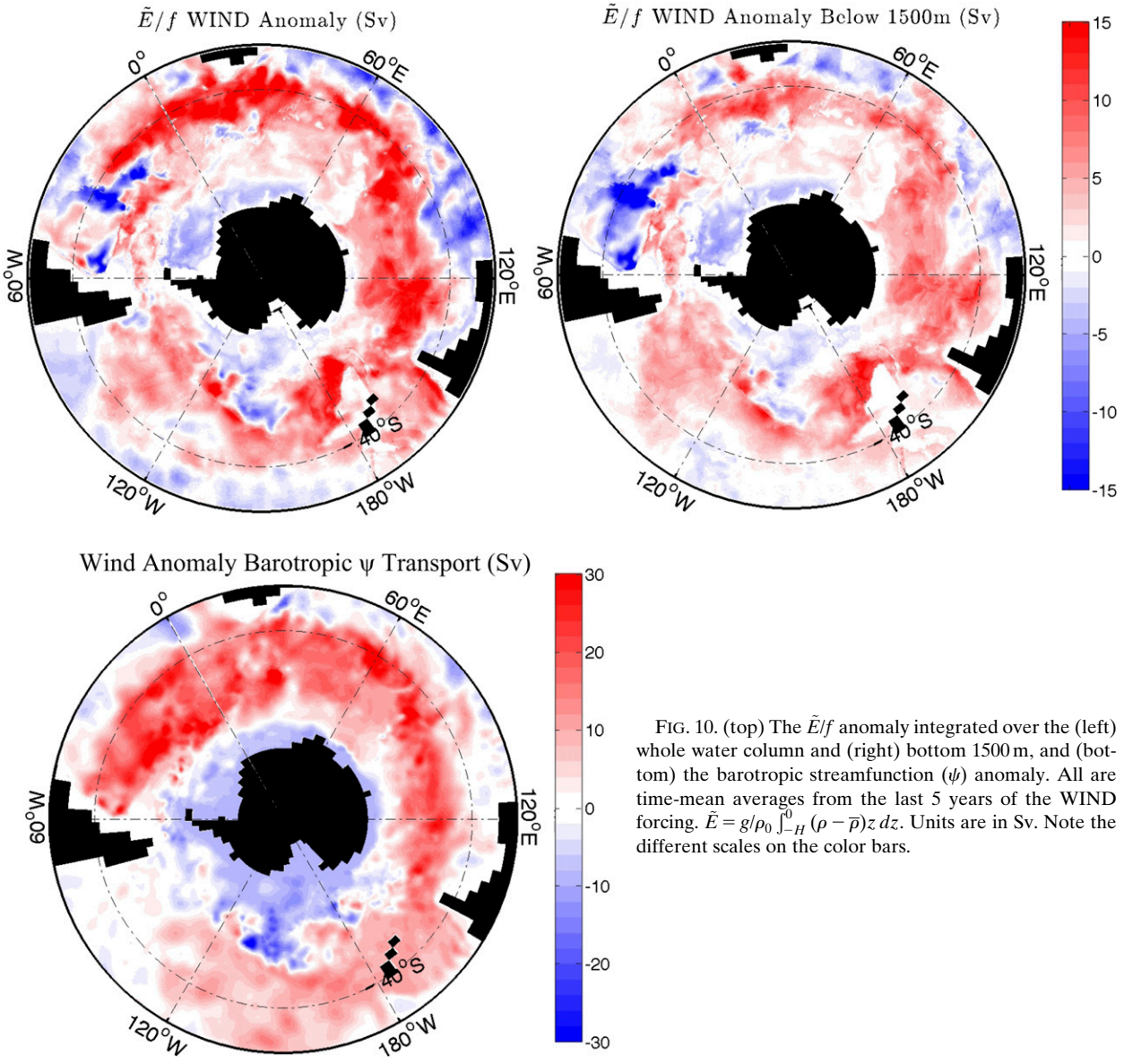

FIG. 10. (top) The $\tilde{E}/f$ anomaly integrated over the (left) whole water column and (right) bottom 1500 m, and (bottom) the barotropic streamfunction (ψ) anomaly. All are time-mean averages from the last 5 years of the WIND forcing. $\tilde{E} = g/\rho_0 \int_{-H}^{0} (\rho - \overline{\rho}) z \, dz$. Units are in Sv. Note the different scales on the color bars.

streamfunction in the Southern Ocean (e.g., Borowski et al. 2002). Here, we confirm the result of Borowski et al. (2002) and argue that in our simulations much of the change in $\Delta\tilde{E}/f$, in response to the changes in winds, results from density changes in the deep Southern Ocean.

4. Summary and conclusions

This study uses a global ocean eddy-permitting climate model to explore the abyssal export of water from the Southern Ocean and its response to the projected twenty-first-century poleward intensification of Southern Ocean wind stress. In the zonally integrated Eulerian framework of the lower-cell MOC, the transient circulation is responsible for roughly one-third of the abyssal transport in the CNTRL simulation. In response to projected twenty-first-century wind stress changes, the maximum intensity of the lower-cell MOC residual transport decreases by roughly 8 Sv, while the transient overturning intensifies by as much as 9 Sv. However, the compensation between opposing meridional flows within similar density classes makes it difficult to decipher how the export of abyssal water from the Southern Ocean is affected by the changing winds in a MOC framework. We find that the equator- and poleward transport components of both the time-mean and transient circulations are enhanced by the changing winds. If one associates the poleward-flowing abyssal water with LCDW and the

equatorward-flowing water as AABW, then these results suggest that twenty-first-century changes in the westerly winds' wind forcing generates large increases in the abyssal transport by the time-mean and transient circulations of both water masses. We note that Stewart and Thompson (2012) find the lower-cell MOC to also be highly sensitive to the strength of the polar easterlies in an idealized channel model.

Purkey and Johnson (2012) argue that the observed warming of AABW between the 1980s and 2000s, revealed as a deepening of abyssal isotherms, implies a global-scale contraction of AABW because volume transports in the ocean interior tend to be aligned with the instantaneous isothermal surfaces. However, while ψ is an effective quantifier of the net meridional flux at a given temperature (Marshall and Radko 2003), changes in the net meridional volume flux do not necessarily imply a change in the export of AABW from the Southern Ocean. Figure 11 shows the zonally averaged Southern Ocean isotherms in the CNTRL and WIND simulations. Note that the isotherms south of 60°S are shallow in response to the WIND forcing, while the lower-cell residual MOC decreases in strength (refer to Fig. 1).

A Lagrangian particle analysis is used to identify the transport pathways of Southern Ocean abyssal water exported into the subtropical basins. Three major pathways equatorward from the Antarctic coast are clearly simulated by the Lagrangian particles: from the Weddell Sea, from the Ross Sea south of New Zealand, and from Prydz Bay near 60°E. The Lagrangian particle analysis of the WIND simulation reveals that the number of abyssal particles exported to the subtropics increases by 11%. In the WIND simulation the number of the abyssal particles sourced in the Weddell Sea increases by up to 25%, and there are also large increases in the Ross Sea and the Cape Darnley polynya along with a general decrease in abyssal particle formation on the western side of the Antarctic Peninsula. When driven by monthly-mean velocity fields, rather than 5-day snapshots, very few the particles in the CNTRL simulation leave the Southern Ocean, which is consistent with the strength of the transient MOC and implies a crucial role for transients in the abyssal transport of water out of the Southern Ocean.

Arguments based on PV budgets identified BPT as a key component maintaining abyssal flow pathways in the Southern Ocean, implying that the input of vorticity into the Southern Ocean by the wind stress curl is balanced by BPT rather than viscous stresses. Coarse-resolution (i.e., >1°) models that require a high horizontal viscosity for numerical stability are likely to have difficulty in accurately simulating the PV balance of the abyssal Southern Ocean vorticity balance. Projected wind stress changes are also found to indirectly influence the Southern Ocean barotropic circulation by modifying the potential energy component of the potential vorticity balance in the abyss.

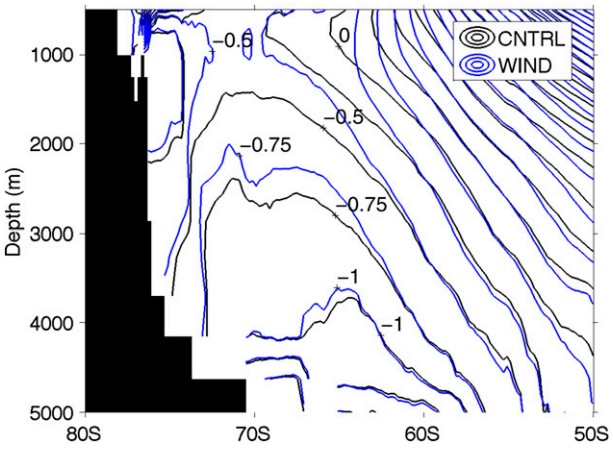

FIG. 11. Zonally averaged Southern Ocean isotherms (°C) averaged over the last 5 years of the CNTRL and WIND simulations.

Acknowledgments. We are grateful for the computing support of Andrew Weaver and the University of Victoria Climate Lab. We also thank J. Fyfe for supplying the projected wind anomalies. This research was supported in part via Grants CE110001028, DE130101336, and FL100100214 from the ARC. Infrastructure support from the University of New South Wales is acknowledged. We thank R. Gerdes for helpful discussions.

APPENDIX

Integrated Budgets of Potential Vorticity

In this section, we briefly review two useful forms of the depth-integrated PV balances, as well as the constraints they impose on the mean large-scale circulation. These balances will be employed for interpreting some of our findings in the next sections. Because we will also analyze the Southern Ocean circulation integrated along time-mean barotropic streamlines of the ACC, the corresponding form of the depth-integrated PV budget is also presented.

Following Hughes and Killworth (1995), it is useful to consider the steady horizontal momentum equation, neglecting nonlinear terms and horizontal friction:

$$\rho_0 f \mathbf{k} \times \mathbf{u} = -\nabla p + \mathbf{T}_z, \tag{A1}$$

where ρ_0 is the reference density, f is the Coriolis parameter, $\mathbf{u}(u, v)$ is the horizontal velocity, p is the

pressure, $\mathbf{T} = (T^x, T^y)$ is the vertical stress, and $T_z = \partial T/\partial z$. Integrating Eq. (A1) vertically and using the continuity equation

$$\nabla \cdot \mathbf{u} + w_z = 0, \tag{A2}$$

with the vertical velocity $w = 0$ at $z = 0$ and $w = -\mathbf{u} \cdot \nabla H$ at the bottom $z = -H(x, y)$, gives

$$-\rho_0 f \nabla \psi = -\int_{-H}^{0} \nabla p \, dz + \tau, \tag{A3}$$

where ψ is the vertically integrated streamfunction and $\tau = (\tau_x, \tau_y)$ is the difference between the surface and the bottom stress (we assume that bottom stress is weak, so that τ is dominated by the wind stress). Using the hydrostatic equation

$$p_z + g\rho = 0, \tag{A4}$$

the vertically integrated pressure gradient can be written as follows:

$$\int_{-H}^{0} \nabla p \, dz = H \nabla p_b + \nabla E, \tag{A5}$$

so that Eq. (A3) takes the form

$$-\rho_0 f \nabla \psi = -H \nabla p_b - \nabla E + \tau, \tag{A6}$$

where p_b is the bottom pressure and $E = g \int_{-H}^{0} \rho z \, dz$ is the potential energy.

Two useful forms of the vorticity equation for the depth-integrated flow can then be obtained. Taking the curl of Eq. (A6) gives

$$\rho_0 \beta \psi_x = J(p_b, H) + \mathbf{k} \cdot \nabla \times \tau, \tag{A7}$$

whereas dividing Eq. (A6) by H and taking the curl gives

$$\rho_0 J(\psi, f/H) = J(E, 1/H) + \mathbf{k} \cdot \nabla \times \frac{\tau}{H}, \tag{A8}$$

where $\beta = f_y$; $J(p_b, H)$ and $J(E, 1/H)$ are the BPT and JEBAR terms, respectively (Sarkisyan and Ivanov 1971). The BPT is closely related to the near-bottom vertical velocity w_b. Taking the curl of Eq. (A1) and integrating it vertically, and using Eq. (A2) and the no normal flow conditions at the surface and through the bottom, gives $\rho_0 f w_b = -J(p_b, H)$ (this also implies that the near-bottom circulation is, under the assumptions made, geostrophic). In the Southern Hemisphere ($f < 0$), an upward w_b implies a northward flow. It may dominate the net meridional transport in regions (e.g., boundary currents) where wind stress curl can be neglected.

The PV balance given by Eq. (A8) is also very useful. First of all, it states that one only needs information about the density field and wind stress, which is available from observations, to estimate the large-scale depth-integrated circulation. Second, it implies that, in the absence of wind stress, in order to force the depth-integrated flow across the contours of f/H = constant, there must be a nonzero JEBAR.

The models used in this study are used to examine both the BPT and JEBAR components, jointly with the pathways of the abyssal circulation in the Southern Ocean. In addition, we will consider the transports in the abyss across the contours of ψ = constant. In this regard, it is useful to note that integrating Eq. (A6) around contours of ψ gives (Hughes and Killworth 1995)

$$\oint_{\psi=\text{constant}} H \nabla p_b \cdot ds = \oint_{\psi=\text{constant}} \tau \cdot ds, \tag{A9}$$

which implies that as long as there is an input of momentum from the wind stress, there must be a nonzero bottom form stress to balance it (Munk and Palmén 1951). Hence, a change in the wind stress along a contour of ψ = constant should result in a change in the near-bottom geostrophic flows. However, the PV balance given by Eq. (A9) does not tell us what the integrated transient circulation in the near-bottom ocean may look like, including in response to changes in the wind stress. This study addresses this question by identifying the transport pathways of the near-bottom circulation in the Southern Ocean in simulations of an ocean eddy-permitting model.

REFERENCES

Antonov, J. I., and Coauthors, 2010: *Salinity.* Vol. 2, *World Ocean Atlas 2009,* NOAA Atlas NESDIS 69, 184 pp.

Borowski, D., R. Gerdes, and D. Olbers, 2002: Thermohaline and wind forcing of a circumpolar channel with blocked geostrophic contours. *J. Phys. Oceanogr.,* **32,** 2520–2540.

Chelton, D. B., M. G. Schlax, R. M. Samelson, and R. A. de Szoeke, 2007: Global observations of large oceanic eddies. *Geophys. Res. Lett.,* **34,** L15606, doi:10.1029/2007GL030812.

Döös, K., J. Nycander, and A. C. Coward, 2008: Lagrangian decomposition of the Deacon cell. *J. Geophys. Res.,* **113,** C07028, doi:10.1029/2007JC004351.

Fyfe, J. C., O. A. Saenko, K. Zickfeld, M. Eby, and A. J. Weaver, 2007: The role of poleward intensifying winds on Southern Ocean warming. *J. Climate,* **20,** 5391–5400.

Hallberg, R., and A. Gnanadesikan, 2006: The role of eddies in determining the structure and response of the wind-driven Southern Hemisphere overturning: Results from the modeling eddies in the Southern Ocean project. *J. Phys. Oceanogr.,* **36,** 2232–2252.

Hughes, C., and P. Killworth, 1995: Effects of bottom topography in the large-scale circulation of the Southern Ocean. *J. Phys. Oceanogr.,* **25,** 2485–2497.

——, and B. de Cuevas, 2001: Why western boundary currents in realistic oceans are inviscid: A link between form stress and bottom pressure torques. *J. Phys. Oceanogr.,* **31,** 2871–2885.

Ito, T., and J. Marshall, 2008: Control of lower-limb overturning circulation in the Southern Ocean by diapycnal mixing and mesoscale transient transfer. *J. Phys. Oceanogr.,* **38,** 2832–2845.

Jacobs, S., 2004: Bottom water production and its links with the thermohaline circulation. *Antarct. Sci.,* **16,** 427–437.

Kistler, R., and Coauthors, 2001: The NCEP–NCAR 50-Year Reanalysis: Monthly means CD-ROM and documentation. *Bull. Amer. Meteor. Soc.,* **82,** 247–267.

Krupitsky, A., and M. Cane, 1997: A two-layer wind-driven ocean model in a multiply connected domain with bottom topography. *J. Phys. Oceanogr.,* **27,** 2395–2404.

Levitus, S., J. Antonov, and T. Boyer, 2005: Warming of the World Ocean, 1955–2003. *Geophys. Res. Lett.,* **32,** L02604, doi:10.1029/2004GL021592.

Locarnini, R. A., A. V. Mishonov, J. I. Antonov, T. P. Boyer, H. E. Garcia, O. K. Baranova, M. M. Zweng, and D. R. Johnson, 2010: *Temperature.* Vol. 1, *World Ocean Atlas 2009,* NOAA Atlas NESDIS 68, 184 pp.

Lumpkin, R., and K. Speer, 2007: Global ocean meridional over turning. *J. Phys. Oceanogr.,* **37,** 2550–2562.

Marshall, J., and T. Radko, 2003: Residual-mean solutions for the Antarctic Circumpolar Current and its associated overturning circulation. *J. Phys. Oceanogr.,* **33,** 2341–2354.

Mazloff, M., P. Heimbach, and C. Wunsch, 2010: An eddy-permitting Southern Ocean state estimate. *J. Phys. Oceanogr.,* **40,** 880–899.

Meehl, G. A., and Coauthors, 2006: Climate change projections for the twenty-first century and climate change commitment in the CCSM3. *J. Climate,* **19,** 2597–2616.

Munk, W. H., and E. Palmén, 1951: Note on the dynamics of the Antarctic Circumpolar Current. *Tellus,* **3,** 53–55.

Nikurashin, M., and G. Vallis, 2011: A theory of deep stratification and overturning circulation in the ocean. *J. Phys. Oceanogr.,* **41,** 485–502.

Oke, R. R., and M. H. England, 2004: Oceanic response to changes in the latitude of the Southern Hemisphere subpolar westerly winds. *J. Climate,* **17,** 1040–1054.

Olbers, D., and V. O. Ivchenko, 2001: On the meridional circulation and balance of momentum in the Southern Ocean of POP. *Ocean Dyn.,* **52,** 79–93.

——, K. Lettmann, and R. Timmermann, 2007: Six circumpolar currents—On the forcing of the Antarctic Circumpolar Current by wind and mixing. *Ocean Dyn.,* **57,** 12–31.

Orsi, A. H., 2010: Recycling bottom waters. *Nat. Geosci.,* **3,** 307–309.

——, G. C. Johnson, and J. L. Bullister, 1999: Circulation, mixing, and production of Antarctic Bottom Water. *Prog. Oceanogr.,* **43,** 55–109.

Paris, C. B., J. Helgers, E. van Sebille, and A. Srinivasan, 2013: Connectivity modeling system: A probabilistic modeling tool for the multi-scale tracking biotic and abiotic variability in the ocean. *Environ. Modell. Software,* **42,** 47–54.

Purkey, S., and G. Johnson, 2012: Global contraction of Antarctic Bottom Water between the 1980s and 2000s. *J. Climate,* **25,** 5830–5844.

Russell, J. L., D. W. Dixon, A. Gnanadesikan, R. J. Stouffer, and J. R. Toggweiler, 2006: The Southern Hemisphere westerlies in a warming world: Propping open the door to the deep ocean. *J. Climate,* **19,** 6382–6390.

Saenko, O. A., A. Sen Gupta, and P. Spence, 2012: On challenges in predicting bottom water transport in the Southern Ocean. *J. Climate,* **25,** 1349–1356.

Santoso, A., M. England, and A. C. Hirst, 2006: Circumpolar deep water circulation and variability in a coupled climate model. *J. Phys. Oceanogr.,* **36,** 1523–1552.

Sarkisyan, A. S., 2006: Forty years of JEBAR—The finding of the joint effect of baroclinicity and bottom relief for the modeling of ocean climatic characteristics. *Izv. Atmos. Oceanic Phys.,* **42,** 534–554.

——, and V. F. Ivanov, 1971: Joint effect of baroclinicity and bottom relief as an important factor in the dynamics of sea currents. *Atmos. Oceanic Phys.,* **7,** 173–188.

Sloyan, S., and S. Rintoul, 2001: The Southern Ocean limb of the global deep overturning circulation. *J. Phys. Oceanogr.,* **31,** 143–173.

Spence, P., O. A. Saenko, M. Eby, and A. J. Weaver, 2009: The Southern Ocean overturning: Parameterized versus permitted eddies. *J. Phys. Oceanogr.,* **39,** 1634–1651.

——, ——, W. Sijp, and M. England, 2012: The role of bottom pressure torques on the interior pathways of North Atlantic Deep Water. *J. Phys. Oceanogr.,* **42,** 110–125.

——, ——, ——, and ——, 2013: North Atlantic climate response to Lake Agassiz drainage at coarse and ocean eddy-permitting resolutions. *J. Climate,* **26,** 2651–2667.

Stewart, A., and A. Thompson, 2012: Sensitivity of the oceans deep overturning circulation to easterly Antarctic winds. *Geophys. Res. Lett.,* **39,** L18604, doi:10.1029/2012GL053099.

Thompson, A., and J. B. Sallée, 2012: Jets and topography: Jet transitions and the impact on transport in the Antarctic Circumpolar Current. *J. Phys. Oceanogr.,* **42,** 956–972.

Thompson, D., S. Solomon, P. Kushner, M. England, K. Grise, and D. Karoly, 2011: Signatures of the Antarctic ozone hole in Southern Hemisphere surface climates change. *Nat. Geosci.,* **4,** 741–749, doi:10.1038/NGEO1296.

van Sebille, E., W. Johns, and L. Beal, 2012: Does the vorticity flux from Agulhas rings control the zonal pathway of NADW across the South Atlantic? *J. Geophys. Res.,* **117,** C05037, doi:10.1029/2011JC007684.

——, P. Spence, M. Mazloff, M. England, S. Rintoul, and O. Saenko, 2013: Abyssal connections of Antarctic Bottom Water in a Southern Ocean state estimate. *Geophys. Res. Lett.,* **40,** 2177–2182, doi:10.1002/grl.50483.

Weaver, A. J., and Coauthors, 2001: The UVic Earth System Climate Model: Model description, climatology and application to past, present and future climates. *Atmos.–Ocean,* **39,** 361–428.